NANO LETTERS

pubs.acs.org/NanoLett Letter

A Single-Molecule Quantum Heat Engine

Serhii Volosheniuk, Riccardo Conte, Eugenia Pyurbeeva, Thomas Baum, Manuel Vilas-Varela, Saleta Fernández, Diego Peña, Herre S. J. van der Zant,* and Pascal Gehring*

Cite This: *Nano Lett.* 2026, 26, 984–989 Read Online

ACCESS | Metrics & More | Article Recommendations | Supporting Information

ABSTRACT: Particle-exchange heat engines operate without moving parts or time-dependent driving, relying solely on static energy-selective transport. Here, we realize a particle-exchange quantum heat engine based on a single diradical molecule, which is only a few nanometers in size. We experimentally investigate its operation at low temperatures and demonstrate that both the power output and efficiency are significantly enhanced by Kondo correlations, reaching up to 53% of the Curzon–Ahlborn limit. These results establish molecular-scale particle-exchange engines as promising candidates for low-temperature applications where extreme miniaturization and energy efficiency are paramount.

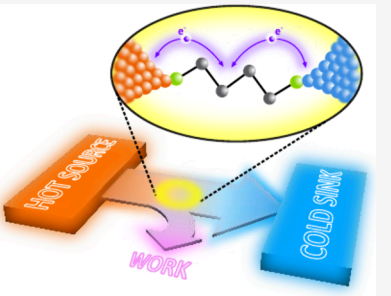

KEYWORDS: *single-molecule heat engine, Kondo effect, molecular electronics, thermopower, particle-exchange heat engine, electromigrated break junctions*

A heat engine converts part of the heat flowing from a hot to a cold reservoir to work (Figure 1a). Classical heat engines exist across a broad range of scales, from macroscopic systems such as steam engines to microscopic devices, including micro-electromechanical,[1] piezoresistive,[2] and single-atom engines.[3] Quantum heat engines exploit discrete energy levels to perform work while interacting with their environment via heat or particle exchange (Figure 1b). These systems must be open and their working medium—analogous to the gas or liquid in classical engines—can consist of quantum particles,[4] spin systems,[5] harmonic oscillators,[6] or single electrons. Furthermore, particle-exchange quantum heat engines are autonomous and operate continuously without time-dependent external driving.

A prominent example for particle-exchange quantum heat engines that relies on single-electron exchange (see Figure 1c) is the quantum dot (QD) heat engine. Its working principle is based on energy filtering, where efficiency is maximized if particle exchange occurs through a narrow energy window—smaller than the thermal energy, k_BT—to suppress entropy generation during transport.[7] Experimentally, quantum dots formed in nanowires, tunnel-coupled to two electron reservoirs, have been demonstrated to be precise energy filters, achieving efficiencies close to the Curzon–Ahlborn limit.[8] Therein, key parameters influencing efficiency are the load resistance[9] and tunnel coupling, which governs charge transport and energy selectivity.[10] Recent studies further emphasize the role of quantum dot degeneracies, which are directly linked to entropy generation,[11,12] and strong electronic correlations,[13−15] in optimizing heat-to-work conversion.

Extending this concept, single molecules have emerged as promising candidates for quantum heat engines. Their unique advantage lies in the ability to chemically tailor their functionality at the molecular level, allowing precise control over the position and width of the effective energy filter, which facilitates the energy conversion process. Unlike inorganic quantum dots, molecules offer additional tunability through their electronic degeneracies, spin ground states, coupling strengths, and internal interference effects, which can be engineered to enhance thermoelectric efficiency.[16−18]

In this work, we explore how strong electron correlations, particularly those giving rise to the Kondo effect, impact the efficiency of a single-molecule heat engine. By performing single-molecule thermoelectric experiments under different load resistors and tuning the intramolecular electron interactions with a magnetic field, we show that the maximum power output of the engine is significantly enhanced in the presence of Kondo correlations. We quantify this enhancement by introducing an asymmetry parameter, σ, which we extract from fits to the experimental data. We show that σ is a reduced characteristic of the internal dynamics of the QD that is responsible for its thermoelectric performance. The understanding obtained in this study is crucial for optimizing heat-to-work conversion in molecular-scale thermoelectric devices, where many-body interactions can significantly alter transport properties. By leveraging molecular design strategies and

Received: September 25, 2025
Revised: November 11, 2025
Accepted: November 12, 2025
Published: November 18, 2025

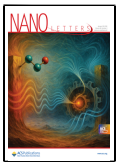

https://doi.org/10.1021/acs.nanolett.5c04824
Nano Lett. 2026, 26, 984–989

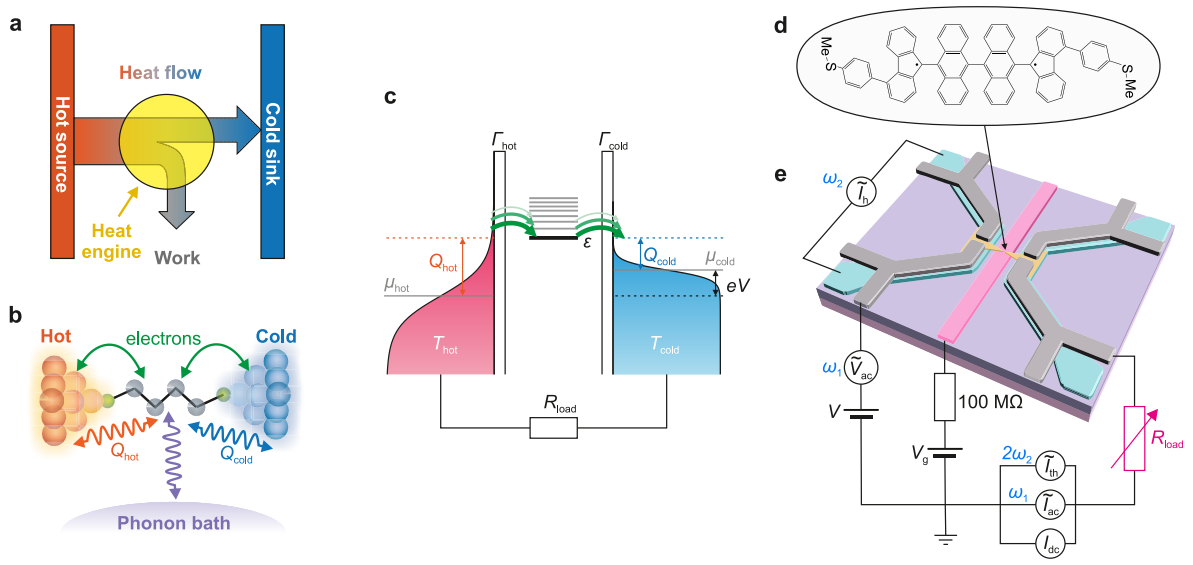

Figure 1. (a) Working principle of a classical heat engine. (b) Principle of a molecular quantum heat engine. Electrons (green arrows) and heat (orange/blue/purple wiggly arrows) are exchanged between the molecule and a hot and cold reservoir. The molecule can furthermore thermalize with its phonon bath. (c) Molecular particle-exchange heat engine. A single molecule (depicted by a ground state in black and (vibrational) excited states in gray) is tunnel-coupled (green arrows) to a hot (left, red) and a cold (right, blue) particle/heat reservoir characterized by Fermi–Dirac distributions (with temperatures T_{hot}, T_{cold} and electrochemical potentials μ_{hot}, μ_{cold}). An electron, driven by the thermal bias, tunneling onto the molecular ground state removes heat, Q_{hot}, from the hot reservoir, converts part of it into useful work eV—which can be optimized by adjusting a load resistor, R_{load}—and transfers the remaining heat, Q_{cold}, to the cold reservoir. (d) Structure of the **SMe-2OS** molecule used in this study. (e) Schematic of the thermopower device showing the back-gate electrode (pink), heaters (light blue), gold bridge (yellow), and gold contacts (gray). The accompanying circuit diagram indicates the terminals used to apply the gate voltage, V_g, dc bias voltage, V, ac bias voltage at frequency ω_1, $V_{ac}(\omega_1)$, and ac heater current at frequency ω_2, $I_h(\omega_2)$, as well as the terminals for measuring the dc current, I_{dc}, ac current, $I_{ac}(\omega_1)$, and thermocurrent, $I_{th}(2\omega_2)$. A load resistor, R_{load}, is connected in series with the molecular heat engine.

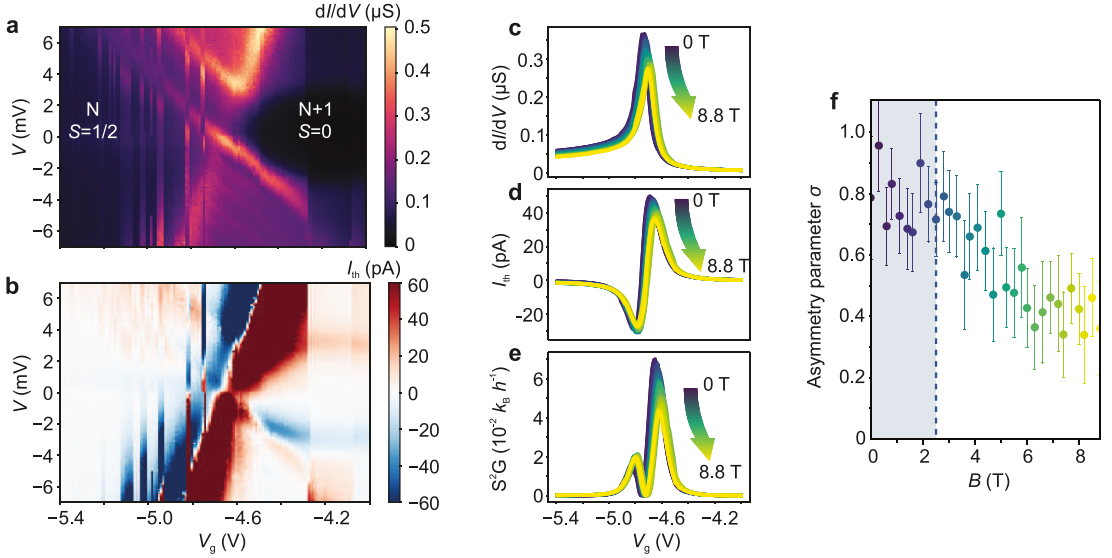

Figure 2. Simultaneously measured stability diagrams of differential conductance (a) and thermocurrent (b). Zero-bias gate traces of differential conductance (c) and thermocurrent (d) at various magnetic fields, showing a shift of the charge degeneracy point toward less negative gate voltages. (e) Evolution of the power factor calculated from (c) and (d) as a function of gate voltage for different magnetic fields. (f) Asymmetry parameter extracted from thermopower measurements as a function of applied magnetic field. Magnetic field strengths are represented by color: dark blue (0 T) transitioning to yellow (8.8 T). The error bars show the confidence intervals of the value of σ from fitting each of the thermocurrent traces to eq 1.

correlation effects, it will be possible to refine energy filtering mechanisms and push the efficiency of nanoscale heat engines to the limits.

The working principle of the single-molecule particle-exchange heat engine studied in this work is illustrated in Figure 1b and c. A single molecule, characterized by its discrete energy levels—specifically, the highest occupied molecular orbital (HOMO) at energy ε_{HOMO} and the lowest unoccupied molecular orbital (LUMO) at energy ε_{LUMO}—is tunnel-coupled to two electron reservoirs with electrochemical potentials μ_{hot} and μ_{cold} on the left (hot) and right (cold)

https://doi.org/10.1021/acs.nanolett.5c04824
Nano Lett. 2026, 26, 984−989

sides, respectively. The tunnel coupling strengths to these reservoirs are denoted as Γ_{hot} and Γ_{cold}.

Typically, in molecular devices, the energy gap $\varepsilon_{HOMO} - \varepsilon_{LUMO}$ is several eV, allowing transport to be effectively described as transitions through the single energy level closest to the Fermi energy (single-level model). The energy required to add an additional electron to this level is given by $\varepsilon = E_{HOMO} - E_{LUMO} - \mu$ (where μ is the chemical potential of the electrode), which accounts for both the charging energy and the quantum level spacings.[19,20] When a temperature bias, $\Delta T = T_{hot} - T_{cold}$, is applied across the molecule, an electronic energy (heat) current J_Q—the phononic heat current can typically be neglected at cryogenic temperatures that are much lower than the vibrational energies of the single molecule—flows from the hot to the cold reservoir, filtered by the molecular level at ε. Simultaneously, this thermal gradient drives a thermoelectric current, I_{th}, against the applied voltage, $V = (\mu_{cold} - \mu_{hot})/e$. Each transferred electron performs electrical work, eV, while transporting heat, extracting $Q_{hot} = \varepsilon - \mu_{hot}$ from the hot reservoir and depositing $Q_{cold} = \varepsilon - \mu_{cold}$ into the cold reservoir. If a load resistor R_{load} is connected in series with the molecular junction, electrical power, $P = I_{th}^2 R_{load}$, is generated. The efficiency of the heat engine is then given by $\eta = \frac{P}{J_Q}$.

, we implement a single-molecule particle-exchange heat engine by incorporating an all-organic **SMe-2OS** molecule (Figure 1d)—a stable diradical which was previously synthesized and studied on surface by scanning tunneling microscopy (STM)[21] (see Methods section in the SI)—into a nanometer-sized junction between two gold electrodes. Here, the thioether SMe($-SCH_3$) end groups are included for anchoring to the Au electrodes. Radical molecules have attracted significant attention in diverse research areas—including synthetic chemistry, spintronics, and nonlinear optics—and have been demonstrated to enhance thermoelectric performance.[18,22] Notably, in our study the molecule's spin ground state can be tuned to $S = 1/2$ by applying a negative gate voltage, V_g, as we will demonstrate later. This junction is formed through the electromigration[23] of a narrow gold constriction (see Methods section in the SI). Our recently developed device architecture[24−26] (Figure 1e) allows for the application and precise measurement of a thermal bias across the junction, even at millikelvin sample temperatures. By simultaneously applying an AC bias voltage, V_{ac}, at frequency ω_1 and an AC heater current, $\tilde{I}_H$, at ω_2, we simultaneously measure both the electrical differential conductance, $dI/dV = \tilde{I}_{ac}/V_{ac}$, at ω_1, and the thermocurrent, I_{th}, at $2\omega_2$ as a function of DC bias voltage, V, and V_g (see Methods section in the SI for details).

Figure 2a and b shows maps of dI/dV and I_{th} as a function of V and V_g. The characteristic hourglass-shaped sequential tunneling regime is observed, a hallmark of Coulomb blockade, with a charge degeneracy point (CDP) at $V_g = -4.7$ V, marking the transition where one electron is removed from the molecule, shifting the system from an $N + 1$ to an N charge ground state. Excited states appear within the sequential tunneling regime and extend into the Coulomb-blocked region of the $N + 1$ state as horizontal lines, characteristic of second-order co-tunneling processes. The response of those features to an external magnetic field indicates that they originate from spin-excited states rather than vibrational excitations. Magnetic field dependence (see SI) reveals that the two spins in the $N + 1$ charge state couple antiferromagnetically, with an exchange coupling strength of $J \approx 3$ meV, confirming that the observed co-tunneling excitation corresponds to a singlet−triplet transition. Additionally, the CDP shifts to less negative energies under an applied magnetic field (see Figure 2c, also the SI), indicating that the ground state on the left side of the CDP has a higher spin than that on the right. This implies a doublet-to-singlet transition upon electron addition with the neutral state of the molecule on the right-hand side of the CDP.

In the N charge ground state—with doublet spin ground state—a horizontal feature at zero bias is visible, which we attribute to the Kondo effect, a many-body phenomenon where a localized spin on the molecule interacts with the conduction electrons of the reservoirs, forming an antiferromagnetically ordered bound state with a binding energy characterized by the Kondo temperature, T_K. Magnetic field dependent measurements of I_{th} can be used to estimate T_K:[14] A universal scaling relation exists between the magnetic field B_c, where the Kondo resonance splits, and B_{th}, where the slope of I_{th} at zero bias changes sign, with $B_{th} \approx B_c = 0.75 k_B T_K/(g\mu_B)$, where g is the g-factor and k_B is the Boltzmann constant.[14] We find (see the SI) $B_{th} = 2.4$ T, yielding a Kondo temperature of $T_K = 4.3$ K. Furthermore, magnetic field sweeps at $V_g = -5.6$ V indicate that the system behaves as a spin-1/2 with a g-factor of 2.

In Figure 2c−e, we present the gate-dependent dI/dV, I_{th}, and the thermoelectric power factor $PF = S^2G = I_{th}^2/\Delta T^2/(dI/dV)$ at various magnetic field strengths, measured with a series resistor of $R_{load} = 100$ kΩ at zero bias voltage. We observe that all three quantities are suppressed as the magnetic field increases: G and S decrease from 363 nS and 336 μV K^{-1} at zero magnetic field to 272 nS and 284 μV K^{-1} at 8.8 T, respectively, resulting in an overall 35% decrease of PF. Additionally, the ratio between the maximum (I_{th+}) and minimum (I_{th-}) thermocurrent decreases from 1.66 at zero field to 1.3 at 8.8 T. This reduction enhances the symmetry of the gate-dependent PF with respect to the CDP.

To quantify the asymmetry of the thermoelectric response around the CDP, we introduce an asymmetry parameter, σ, extracted by fitting the gate-voltage dependence of the thermocurrent $I_{th}(V_g)$ to the form derived in ref 11 (see Section 7.2 in the SI):

$$I_{th}(V_g) = A\varepsilon\frac{dT}{T^2}f(\varepsilon - T\sigma)(1 - f(\varepsilon)) \quad (1)$$

In the regime of weak electron−electron interactions, where the Onsager symmetry (eq 1, SI) applies, σ can be interpreted as the entropy change associated with adding an electron to the system. In the Kondo regime, the situation changes: conductance develops a plateau only on one side of the CDP, signaling breakdown of Onsager symmetry. Moreover, charge transport no longer occurs through sequential tunneling via the level at ε, but through higher-order co-tunneling processes. In this regime, σ no longer reflects a thermodynamic entropy difference but instead serves as a phenomenological measure of the asymmetry in the thermoelectric signal.

However, despite its lack of an immediate physical interpretation, σ remains an appropriate parameter for characterizing the performance of the device as a heat engine,

https://doi.org/10.1021/acs.nanolett.5c04824
Nano Lett. 2026, 26, 984−989

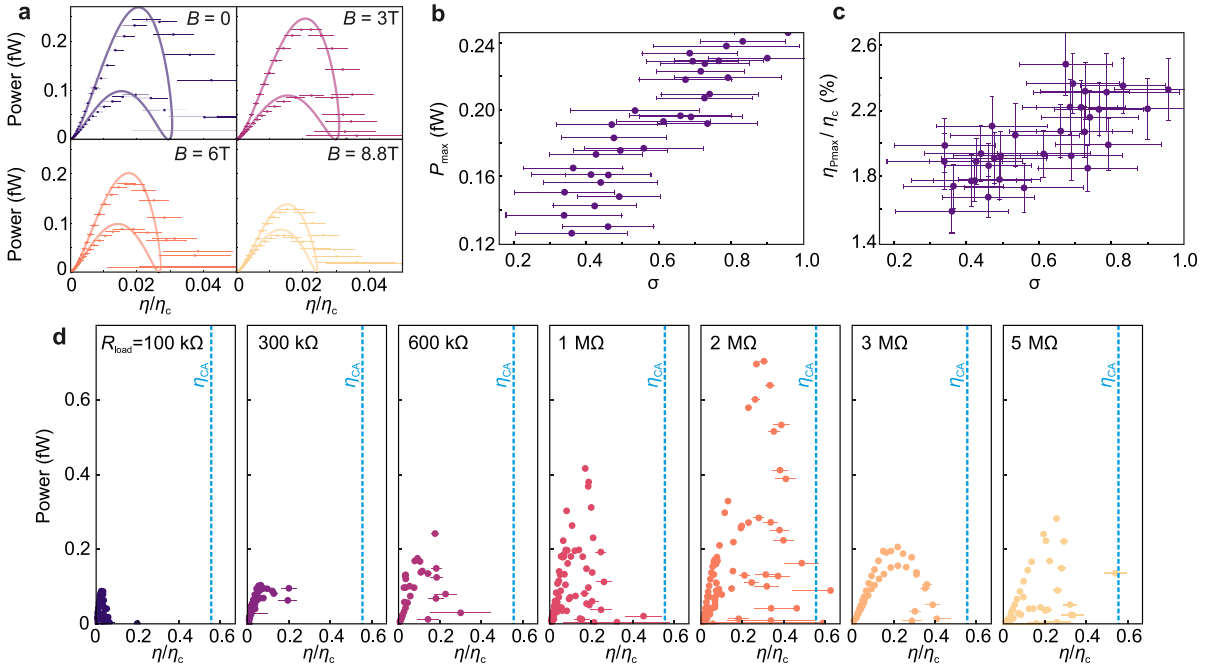

Figure 3. (a) Experimental and theoretical parametric plot of power output as a function of extracted efficiency at different magnetic fields. Here, each point is taken at a different gate voltage. (b) Maximum power output and (c) efficiency at maximum power as a function of asymmetry parameter. (d) Power output as a function of efficiency for different load resistors. The error bars originate from fitting uncertainties, in the determination of either σ or ΔT, which, in turn, affects heat flow and η_C.

as the form of conductance and thermocurrent in ref 11 gives an adequate description of G and I_{th} in the gate voltage range of nonzero thermocurrent, where the heat engine operates. The Kondo effect-induced deviation in conductance is most prominent where the thermocurrent is close to zero (see Figure 2b,c). We display the asymmetry parameter as a function of the magnetic field in Figure 2f. The data indicate that σ remains approximately constant for magnetic fields below $B \approx B_{th}$. For $B > B_{th}$, σ exhibits a decrease with B.

In the following, we calculate the power output, P, and efficiency, η, of the molecular heat engine from measurements performed with different R_{load} values and under different magnetic fields. While it is possible to estimate the thermal conductivity of quantum dots experimentally,[27] our device design does not permit direct measurements. Therefore, we estimate the heat flow, J_Q, using the phenomenological model, valid for small energy level spacings (see the SI). All required input parameters (tunnel couplings to reservoirs, Γ_{hot} and Γ_{cold}, ΔT) were obtained from fits to the experimental conductance and thermocurrent data (see the SI).

Figure 3a shows P as a function of η normalized by the Carnot efficiency $\eta_C = 1 - T_C/T_H$ with a series resistor of R_{load} = 100 kΩ recorded at different B-fields. Each data point in the plot corresponds to a specific configuration of the molecular level relative to the electrochemical potentials μ_h and μ_c of the leads (i.e., different gate voltage). By adjusting ε through changing the gate voltage, it is possible to favor either maximum thermoelectric efficiency, η, or maximum output power, P_{max}. From these data, we extract the maximum power output, P_{max}, and the efficiency at maximum power, $\eta_{P_{max}}$, which are plotted in Figures 3b,c as a function of the asymmetry parameter σ. We observe that $\eta_{P_{max}}$ reaches approximately 2.3% of the Curzon−Ahlborn limit, $\eta_{CA} = 1 - \sqrt{T_c/T_h}$, a benchmark for endoreversible heat engines. Importantly, $\eta_{P_{max}}$ exhibits a clear increase with increasing σ (decreasing magnetic field strength), indicating an impact of Kondo correlations on thermodynamic performance, as will be discussed below. In addition, we find that $\eta_{P_{max}}$ can be further optimized by tuning the external load resistance, R_{load}, as shown in Figure 3d. A maximum of $\eta_{P_{max}} \approx 0.53\eta_{CA}$ is achieved for R_{load} = 2MΩ. For larger R_{load} values, the efficiency decreases again.

Our measurements show that the application of a magnetic field reduces the output power of the molecular heat engine by approximately 50%. Magnetic field-induced changes in thermoelectric performance have previously been reported for radical molecules,[11] where they were attributed to variations in the spin entropy of different charge states. However, this model does not account for our observations. Based on the observed asymmetry in the thermocurrent, one would expect a higher entropy in the $N + 1$ charge state than in the N state. Yet, our transport data indicate a doublet-to-singlet transition upon adding an electron, i.e., a transition from an N-electron doublet to an $(N + 1)$-electron singlet ground state, implying the opposite entropy trend. We therefore attribute the observed thermocurrent asymmetry—and its magnetic field dependence—to Kondo correlations.

Asymmetric thermoelectric line shapes arising from spin-correlated transport have been reported in quantum dots formed in two-dimensional electron gases,[28] semiconductor nanowires,[13] and gold nanoparticle junctions.[29] In the weak electronic coupling regime, where the magnetic field exceeds the Kondo temperature ($B \gg B_{th}$) and spin correlations are suppressed, the thermovoltage exhibits both positive and negative contributions near the conductance peaks. This behavior arises from two distinct transport mechanisms: (1) a linear increase in thermovoltage at the center of a conductance peak due to sequential tunneling and (2) a rapid decrease between peaks associated with co-tunneling

https://doi.org/10.1021/acs.nanolett.5c04824
Nano Lett. 2026, 26, 984−989

processes. In this regime, our data qualitatively follow the negative parametric derivative of the conductance, as described by Mott's relation (see SI). In contrast, in the presence of strong spin correlations, our data—consistent with earlier studies[28]—show clear deviations from Mott's prediction. These deviations lead to an enhanced thermocurrent I_{th} and, consequently, an increased output power of the molecular heat engine for $B < B_{th}$.

The enhanced thermoelectric output observed in our single-molecule heat engine in the Kondo regime likely originates from the sharp many-body resonance that forms near the Fermi level due to strong electron correlations. This resonance significantly modifies the transmission function, acting as a narrow energy filter for charge carriers. The thermoelectric response is enhanced when the resonance is slightly asymmetric, with respect to the chemical potential, and tuned to minimize entropy production by charge transport. Such asymmetry and tuning can arise from gate voltage control or asymmetric coupling to the electrodes and are known to amplify the Seebeck coefficient and thermoelectric power output, as shown in theoretical studies based on the Anderson impurity model.[30,31]

We further analyze the performance of the molecular heat engine in the Kondo regime by comparing numerical simulations (see Section 7.3 in the SI), which incorporate the asymmetry parameter σ, to experimental data. The comparison reveals that increasing σ enhances heat engine performance: it leads to higher maximum power output, improved power generation in nonoptimized regimes, nearly constant efficiency at maximum power, and a slight increase in the maximum achievable efficiency.

We have demonstrated a single-molecule particle-exchange heat engine based on a diradical molecule operating at cryogenic temperatures in which energy filtering is governed by a discrete molecular orbital strongly renormalized by many-body interactions. By combining electrical and thermoelectric measurements under tunable magnetic fields, we revealed that Kondo correlations, a hallmark of strong electron−electron interactions, significantly enhance the power output of the heat engine. Strikingly, we find that in the presence of Kondo correlations, the molecular engine achieves an efficiency of approximately 53% of the Curzon−Ahlborn limit, a performance close to the best quantum dot heat engines reported to date. Our findings show that quantum many-body effects, often regarded as detrimental to coherent transport, can be harnessed to boost thermoelectric performance at the nanoscale. Looking forward, our work opens new pathways to engineer high-performance molecular heat engines by tuning spin states, electronic degeneracies, and correlation effects via chemical design and external fields.

■ ASSOCIATED CONTENT

Data Availability Statement

The complete data set of experiments with description and code are available free of charge.

Supporting Information

The Supporting Information is available free of charge at https://pubs.acs.org/doi/10.1021/acs.nanolett.5c04824.

Methods section (device fabrication, molecular data, measurement protocol); DC stability diagram; characterization of Kondo peak, inelastic tunneling spectra at the right of the charge degeneracy point (CDP), evolution of CDP movement in a magnetic field, and thermocurrent at zero bias; theoretical considerations for heat flow estimation; description of data analysis and fitting protocol (PDF)

■ AUTHOR INFORMATION

Corresponding Authors

Herre S. J. van der Zant − *Kavli Institute of Nanoscience, Delft University of Technology, Delft 2628 CJ, The Netherlands;* orcid.org/0000-0002-5385-0282; Email: h.s.j.vanderzant@tudelft.nl

Pascal Gehring − *IMCN/NAPS, Université Catholique de Louvain, Louvain-la-Neuve 1348, Belgium;* orcid.org/0000-0002-7073-9922; Email: pascal.gehring@uclouvain.be

Authors

Serhii Volosheniuk − *Kavli Institute of Nanoscience, Delft University of Technology, Delft 2628 CJ, The Netherlands*

Riccardo Conte − *Kavli Institute of Nanoscience, Delft University of Technology, Delft 2628 CJ, The Netherlands*

Eugenia Pyurbeeva − *The Fritz Haber Center for Theoretical Chemistry, Institute of Chemistry, The Hebrew University of Jerusalem, Jerusalem 9190401, Israel*

Thomas Baum − *Kavli Institute of Nanoscience, Delft University of Technology, Delft 2628 CJ, The Netherlands;* orcid.org/0000-0003-2802-5384

Manuel Vilas-Varela − *Centro Singular de Investigación en Química Biolóxica e Materiais Moleculares (CiQUS) and Departamento de Química Orgánica, Universidade de Santiago de Compostela, Santiago de Compostela 15782, Spain;* orcid.org/0000-0002-6768-5441

Saleta Fernández − *Centro Singular de Investigación en Química Biolóxica e Materiais Moleculares (CiQUS) and Departamento de Química Orgánica, Universidade de Santiago de Compostela, Santiago de Compostela 15782, Spain*

Diego Peña − *Centro Singular de Investigación en Química Biolóxica e Materiais Moleculares (CiQUS) and Departamento de Química Orgánica, Universidade de Santiago de Compostela, Santiago de Compostela 15782, Spain; Oportunius, Galician Innovation Agency (GAIN), Santiago de Compostela 15702, Spain;* orcid.org/0000-0003-3814-589X

Complete contact information is available at: https://pubs.acs.org/10.1021/acs.nanolett.5c04824

Author Contributions

S.V. fabricated the devices, performed the electrical/thermoelectric measurements, validated and analyzed the experimental data, and supervised R.C. on fabrication of devices and performing measurements. R.C. performed the electrical/thermoelectric measurements and analyzed the experimental data. E.P. implemented a theoretical model for heat flow calculations and supported data analysis. S.F., M.V.-V., and D.P. synthesized the molecule. T.B. supported the experiment. P.G. and H.S.J.v.d.Z. conceived and initiated the project. The manuscript was written through the contributions of all authors. All authors have approved the final version of the manuscript.

Notes

The authors declare no competing financial interest.

https://doi.org/10.1021/acs.nanolett.5c04824
Nano Lett. 2026, 26, 984−989

■ ACKNOWLEDGMENTS

The authors acknowledge the financial support from the EU (FET-767187-QuIET, ERC-StG-10104144-MOUNTAIN, ERC Synergy Grant MolDAM (no. 951519)), from the F.R.S.-FNRS of Belgium (FNRS-CQ-1.C044.21-SMARD, FNRS-CDR-J.006823.F1-SiMolHeat), from The Netherlands Organisation for Scientific Research (NWO/OCW), as part of the Frontiers of Nanoscience program, from SPRING (EU Horizon 2020, project 863098), from Atypical (EU Pathfinder, project 101099098), from the Spanish Agencia Estatal de Investigacion (PID2022-140845OB-C62), from the Xunta de Galicia (Centro de Investigacion do Sistema Universitario de Galicia, 2023-2027, ED431G 2023/03), and the from European Union (European Regional Development FundERDF). E.P. is grateful to the Azrieli Foundation for the award of an Azrieli Fellowship. The authors thank Alessandra Canetta for creating the Table of Contents graphic.

■ REFERENCES

(1) Whalen, S.; Thompson, M.; Bahr, D.; Richards, C.; Richards, R. Design, fabrication and testing of the P3 micro heat engine. *Sensors and Actuators A: Physical* **2003**, *104*, 290−298.
(2) Steeneken, P. G.; Le Phan, K.; Goossens, M. J.; Koops, G. E. J.; Brom, G. J. A. M.; van der Avoort, C.; van Beek, J. T. M. Piezoresistive heat engine and refrigerator. *Nat. Phys.* **2011**, *7*, 354−359.
(3) Roßnagel, J.; Dawkins, S. T.; Tolazzi, K. N.; Abah, O.; Lutz, E.; Schmidt-Kaler, F.; Singer, K. A single-atom heat engine. *Science* **2016**, *352*, 325−329.
(4) Quan, H. T. Quantum thermodynamic cycles and quantum heat engines. II. *Phys. Rev. E* **2009**, *79*, 041129.
(5) Feldmann, T.; Kosloff, R. Quantum four-stroke heat engine: Thermodynamic observables in a model with intrinsic friction. *Phys. Rev. E* **2003**, *68*, 016101.
(6) Rezek, Y.; Kosloff, R. Irreversible performance of a quantum harmonic heat engine. *New J. Phys.* **2006**, *8*, 83.
(7) Mahan, G. D.; Sofo, J. O. The best thermoelectric. *Proc. Natl. Acad. Sci. U. S. A.* **1996**, *93*, 7436−7439.
(8) Josefsson, M.; Svilans, A.; Burke, A. M.; Hoffmann, E. A.; Fahlvik, S.; Thelander, C.; Leijnse, M.; Linke, H. A quantum-dot heat engine operating close to the thermodynamic efficiency limits. *Nat. Nanotechnol.* **2018**, *13*, 920−924.
(9) Josefsson, M.; Svilans, A.; Linke, H.; Leijnse, M. Optimal power and efficiency of single quantum dot heat engines: Theory and experiment. *Phys. Rev. B* **2019**, *99*, 235432.
(10) Verma, S.; Singh, A. A Strongly Correlated Quantum Dot Heat Engine with Optimal Performance: A Nonequilibrium Green's Function Approach. *physica status solidi (b)* **2023**, *260*, 2200608.
(11) Pyurbeeva, E.; Hsu, C.; Vogel, D.; Wegeberg, C.; Mayor, M.; van der Zant, H.; Mol, J. A.; Gehring, P. Controlling the Entropy of a Single-Molecule Junction. *Nano Lett.* **2021**, *21*, 9715−9719.
(12) Pyurbeeva, E.; Mol, J. A.; Gehring, P. Electronic measurements of entropy in meso- and nanoscale systems. *Chemical Physics Reviews* **2022**, *3*, 041308.
(13) Svilans, A.; Josefsson, M.; Burke, A. M.; Fahlvik, S.; Thelander, C.; Linke, H.; Leijnse, M. Thermoelectric Characterization of the Kondo Resonance in Nanowire Quantum Dots. *Phys. Rev. Lett.* **2018**, *121*, 206801.
(14) Hsu, C.; Costi, T. A.; Vogel, D.; Wegeberg, C.; Mayor, M.; van der Zant, H. S. J.; Gehring, P. Magnetic-Field Universality of the Kondo Effect Revealed by Thermocurrent Spectroscopy. *Phys. Rev. Lett.* **2022**, *128*, 147701.
(15) Volosheniuk, S.; Bouwmeester, D.; Vogel, D.; Wegeberg, C.; Hsu, C.; Mayor, M.; van der Zant, H. S. J.; Gehring, P. Enhancing thermoelectric output in a molecular heat engine utilizing Yu-Shiba-Rusinov bound states. *Nat. Commun.* **2025**, *16*, 3279.
(16) Peng, W.; Chen, N.; Xie, Y.; Ma, L.; Lü, J.-T.; Li, Y. Heteroatom engineering for enhancing the thermoelectric power factor of molecular junctions. *J. Mater. Chem. A* **2025**, *13*, 15222−15231.
(17) Ma, L.; Nian, L.-L.; Lü, J.-T. Design and optimization of a heat engine based on a porphyrin single-molecule junction with graphene electrodes. *Phys. Rev. B* **2020**, *101*, 045410.
(18) Park, S.; Jang, J.; Tanaka, Y.; Yoon, H. J. High Seebeck Coefficient Achieved by Multinuclear Organometallic Molecular Junctions. *Nano Lett.* **2022**, *22*, 9693−9699.
(19) Gehring, P.; Thijssen, J. M.; van der Zant, H. S. J. Single-molecule quantum-transport phenomena in break junctions. *Nature Reviews Physics* **2019**, *1*, 381−396.
(20) Pyurbeeva, E.; Mol, J. A. A Thermodynamic Approach to Measuring Entropy in a Few-Electron Nanodevice. *Entropy* **2021**, *23*, 640.
(21) Vegliante, A.; Fernández, S.; Ortiz, R.; Vilas-Varela, M.; Baum, T. Y.; Friedrich, N.; Romero-Lara, F.; Aguirre, A.; Vaxevani, K.; Wang, D.; Garcia Fernandez, C.; van der Zant, H. S. J.; Frederiksen, T.; Peña, D.; Pascual, J. I. Tuning the Spin Interaction in Nonplanar Organic Diradicals through Mechanical Manipulation. *ACS Nano* **2024**, *18*, 26514−26521.
(22) Yang, C.; Chen, Z.; Yu, C.; Cao, J.; Ke, G.; Zhu, W.; Liang, W.; Huang, J.; Cai, W.; Saha, C.; Sabuj, M. A.; Rai, N.; Li, X.; Yang, J.; Li, Y.; Huang, F.; Guo, X. Regulation of quantum spin conversions in a single molecular radical. *Nat. Nanotechnol.* **2024**, *19*, 978−985.
(23) O'Neill, K.; Osorio, E. A.; van der Zant, H. S. J. Self-breaking in planar few-atom Au constrictions for nanometer-spaced electrodes. *Appl. Phys. Lett.* **2007**, *90*, 133109.
(24) Gehring, P.; van der Star, M.; Evangeli, C.; Le Roy, J. J.; Bogani, L.; Kolosov, O. V.; van der Zant, H. S. J. Efficient heating of single-molecule junctions for thermoelectric studies at cryogenic temperatures. *Appl. Phys. Lett.* **2019**, *115*, 073103.
(25) Gehring, P.; Sowa, J. K.; Hsu, C.; de Bruijckere, J.; van der Star, M.; Le Roy, J. J.; Bogani, L.; Gauger, E. M.; van der Zant, H. S. J. Complete mapping of the thermoelectric properties of a single molecule. *Nat. Nanotechnol.* **2021**, *16*, 426−430.
(26) Volosheniuk, S.; Bouwmeester, D.; Hsu, C.; van der Zant, H. S. J.; Gehring, P. Implementation of SNS thermometers into molecular devices for cryogenic thermoelectric experiments. *Appl. Phys. Lett.* **2023**, *122*, 103501.
(27) Dutta, B.; Peltonen, J. T.; Antonenko, D. S.; Meschke, M.; Skvortsov, M. A.; Kubala, B.; König, J.; Winkelmann, C. B.; Courtois, H.; Pekola, J. P. Thermal Conductance of a Single-Electron Transistor. *Phys. Rev. Lett.* **2017**, *119*, 077701.
(28) Scheibner, R.; Buhmann, H.; Reuter, D.; Kiselev, M. N.; Molenkamp, L. W. Thermopower of a Kondo Spin-Correlated Quantum Dot. *Phys. Rev. Lett.* **2005**, *95*, 176602.
(29) Dutta, B.; Majidi, D.; García Corral, A.; Erdman, P. A.; Florens, S.; Costi, T. A.; Courtois, H.; Winkelmann, C. B. Direct Probe of the Seebeck Coefficient in a Kondo-Correlated Single-Quantum-Dot Transistor. *Nano Lett.* **2019**, *19*, 506−511.
(30) Costi, T. A.; Zlatić, V. Thermoelectric transport through strongly correlated quantum dots. *Phys. Rev. B* **2010**, *81*, 235127.
(31) Dong, B.; Lei, X. L. Effect of the Kondo correlation on the thermopower in a quantum dot. *J. Phys.: Condens. Matter* **2002**, *14*, 11747.

https://doi.org/10.1021/acs.nanolett.5c04824
Nano Lett. 2026, 26, 984−989